A Simple Frequency Diversity Scheme for Ultra-Reliable Communications in Ground Reflection Scenarios

Karl-Ludwig Besser, *Graduate Student Member, IEEE*, Eduard A. Jorswieck, *Fellow, IEEE*, and Justin P. Coon, *Senior Member, IEEE*

arXiv:2206.13459v1 [cs.IT] 27 Jun 2022

***Abstract*—We consider a two-ray ground reflection scenario with unknown distance between transmitter and receiver. By utilizing two frequencies in parallel, we can mitigate possible destructive interference and ensure ultra-reliability with only very limited knowledge at the transmitter. In order to achieve this ultra-reliability, we optimize the frequency spacing such that the worst-case receive power is maximized. Additionally, we provide an algorithm to calculate the optimal frequency spacing. Besides the receive power, we also analyze the achievable rate and outage probability. It is shown that the frequency diversity scheme achieves a significant improvement in terms of reliability over using a single frequency. In particular, we demonstrate the effectiveness of the proposed approach by a numerical simulation of a unmanned aerial vehicle (UAV) flying above flat terrain.**

***Index Terms*—Ultra-reliable communications, Two-ray ground reflection, Frequency diversity, Outage probability, Worst-case design.**

I. Introduction

Reliability is a major requirement for many modern applications of wireless communication systems [1], [2]. In particular, this includes autonomous vehicles, e.g., self-driving cars and unmanned aerial vehicles (UAVs). It is therefore of great interest to develop techniques, which enable ultra-reliable communications, e.g., assuring low outage probabilities below 10^{-5} [3]. This is especially important for scenarios where only limited information, e.g., channel state information (CSI), is available at the transmitter, e.g., due to high mobility or in frequency-division duplex (FDD) systems.

It has been observed that negative dependency between channel gains can significantly improve reliability [4]–[6]. The basic idea is to establish multi-link diversity and ensure that always one communication link is available, if the others fail. We will apply this idea in the following to develop a simple frequency diversity scheme that enables ultra-reliable communications in two-ray ground reflection scenarios. In this two-ray model, it is assumed that only one significant multipath component exists in addition to a line-of-sight (LoS) connection. The second component is typically caused by a single reflection on a ground surface. This could occur in flat outdoor terrain [7], on large concrete areas, e.g., airports [8], and for a UAV flying above water [9]–[11]. It has also been observed that the two-ray model can be appropriate for vehicle-to-vehicle (V2V) communication scenarios [12], [13]. In particular, this includes high frequency bands like millimeter wave (mmWave) [14]–[18].

In general, the curvature of the Earth's surface needs to be considered for long-distance outdoor settings and accurate models like the curved-Earth model [10], [19], [20] exist. However, when considering relatively short distances, the flat-Earth model is a valid approximation [10], [20], which we adopt throughout this work.

When varying the distance between transmitter and receiver, the relative phase of the two received signal components varies and they may interfere constructively or destructively. A destructive interference causes a drop of receive power, which in turn could cause an outage of the communication link. In order to mitigate drops of the signal power on one frequency, a second frequency can be used in parallel. The use of multiple frequencies in parallel to create diversity and improve the reliability in ground reflection scenarios has already been proposed in [4] and [21]. In [22], it is analyzed and experimentally verified that frequency diversity improves the performance of distance measurements in outdoor ground reflection scenarios. Instead of using multiple frequencies in parallel, it was shown experimentally in [8] that using multiple antennas and carefully choosing the spacing between them can also improve the received power.

A similar problem setup of multipath fading mitigation is considered in [23], where the authors consider reconfigurable intelligent surface (RIS) as solution method. However, such surfaces need to be deployed first and might not always be available, e.g., in the considered large-scale outdoor scenarios.

In this work, we focus on worst-case design for a frequency diversity system with very limited information at the communication parties. We assume that the transmitter does not know the exact distance to the receiver but only has knowledge about lower and upper bounds on the possible distances, e.g., based on a rough estimation of the user positions. In particular, we optimize the spacing between the two frequencies such that the worst-case receive power in the geographical range is maximized. This can enable ultra-reliability without the need of perfect CSI at the transmitter.

Karl-Ludwig Besser and Eduard A. Jorswieck are with the Institute of Communications Technology, Technische Universität Braunschweig, 38106 Braunschweig, Germany (email: {k.besser, e.jorswieck}@tu-bs.de).

Justin P. Coon is with the Department of Engineering Science, University of Oxford, Oxford OX1 3PJ, U. K. (email: justin.coon@eng.ox.ac.uk).

The work of E. Jorswieck is partly supported by the Federal Ministry of Education and Research Germany (BMBF) as part of the 6G Research and Innovation Cluster 6G-RIC under Grant 16KISK020K. The work of J. Coon is supported by the EPSRC under grant number EP/T02612X/1.

Our main contributions and the outline of the manuscript are summarized as follows.

- We analyze the worst-case received power for a two-ray ground reflection model with unknown distance between transmitter and receiver when employing only a single frequency. (Section III)
- We analyze the received power and provide a lower bound when employing two frequencies in parallel. (Section IV)
- In particular, we determine the optimal frequency spacing which maximizes the worst-case receive power. (Theorem 2)
- An algorithm and its implementation is provided to calculate the optimal frequency spacing for given system parameters. (Algorithm 1 and [24])
- In addition to the receive power, we also analyze the achievable rate (Section V) and outage probability (Section VI).

Notation

An overview of the most commonly used variable notation can be found in Table I.

Table I
Notation of the Most Commonly Used Variables and System Parameters

d	Distance between transmitter and receiver (on the ground) [m]
h_{Tx}	Height of the transmitter [m]
h_{Rx}	Height of the receiver [m]
ℓ	Length of the LoS path [m]
$\tilde{\ell}$	Total length of the reflection path [m]
c	Speed of light $= 299\,792\,458\,\mathrm{m/s}$
$\omega = 2\pi f$	(Angular) frequency ([rad/s]) [Hz]
G_{los}	Overall antenna gain for the direction of the LoS path [dB]
G_{ref}	Overall antenna gain for the direction of the reflected path [dB]
$\rho = \sqrt{G_{ref}/G_{los}}$	Relative gain for the direction of the reflected path
P_t	Transmit power [W]
P_r	Receive power [W]
$\underline{P_r}$	Lower bound of the receive power [W]
d_k	Distance at which the k-th local minimum of the receive power occurs [m]
$\Delta\omega = 2\pi\Delta f = \omega_2 - \omega_1$	(Angular) frequency spacing ([rad/s]) [Hz]
$\Delta\omega_\pi$	First maximum of $\underline{P_r}(d, \Delta\omega)$ with respect to $\Delta\omega$ [rad/s]
$\widetilde{\Delta\omega}$	First minimum of $\underline{P_r}(d, \Delta\omega)$ with respect to $\Delta\omega$ [rad/s]
R	Rate [bit/s]
B	Bandwidth [Hz]
F	Receiver noise figure [dB]
N_0	Noise spectral density [dBm/Hz]

In order to simplify the notation, we will omit variables on which functions depend when their value is clear from the context, e.g., we will write $f(x)$ instead of $f(x, y)$ when the value of y is fixed.

Since the angular frequency $\omega = 2\pi f$ is a simple scaling of the frequency f, we will treat them somewhat interchangeably. Especially for calculations, it is more convenient to use ω, while f is relevant for actual system design. We will therefore use the frequency f for the numerical examples while expressing all formulas in terms of the angular frequency ω.

For a random variable X, we use F_X and p_X for its cumulative distribution function (CDF) and probability density function (PDF), respectively. The expectation is denoted by $\mathbb{E}$ and the probability of an event by $\Pr$. The uniform distribution on the interval $[a, b]$ is denoted as $\mathcal{U}[a, b]$.

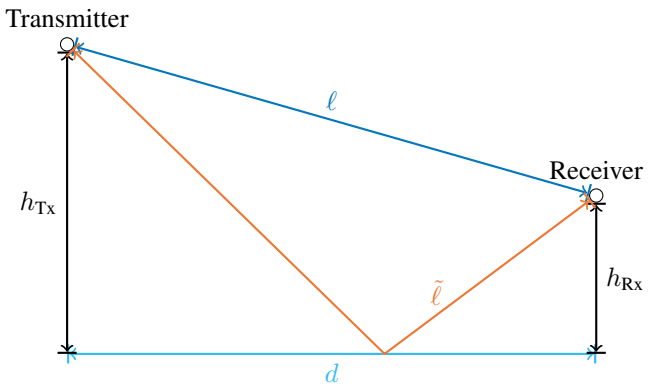


Figure 1. Geometrical model of the considered two-ray ground reflection scenario. The transmitter is placed at height h_{Tx} above the ground. The receiver is located at height h_{Rx} at a (ground) distance d away from the transmitter. The LoS path and reflection path have lengths ℓ and $\tilde{\ell}$, respectively.

II. System Model and Problem Formulation

Throughout the following, we consider the classical two-ray ground reflection model [25, Chap. 4.6]. In this scenario, the propagation environment is approximated as a plane reflecting ground surface. A single-antenna transmitter is located at height h_{Tx} above the ground. At distance d, the single-antenna receiver is placed at height h_{Rx}. This geometrical model is depicted in Fig. 1.

Based on the setup, it can be seen that the transmitted signal is propagated via two separate paths to the receiver. On the one hand, there exists a LoS propagation with path length ℓ. On the other hand, the signal is also reflected by the ground, which leads to the second component. The total length of the second ray is $\tilde{\ell}$. Finally, these two components superimpose at the receiver.

From basic trigonometric considerations, the path lengths can be calculated as

$$\ell^2 = (h_{\mathrm{Tx}} - h_{\mathrm{Rx}})^2 + d^2 \tag{1}$$

$$\tilde{\ell}^2 = (h_{\mathrm{Tx}} + h_{\mathrm{Rx}})^2 + d^2\,. \tag{2}$$

When transmitting on a single frequency $\omega = 2\pi f$, the received power P_r at distance d is given in (3) at the top of the next page [25, Chap. 4.6], [26, Chap. 2.1.2], [4, Eq. (2)] with the additional notation from Table I[1].

[1]In order to simplify the notation, we will omit variables on which functions depend when their value is clear from the context, e.g., we will write $P_r(d)$ instead of $P_r(d, \omega)$ when the value of ω is fixed.

$$P_r(d,\omega;h_{\text{Tx}},h_{\text{Rx}},P_t)=P_t\left(\frac{c}{2\omega}\right)^2\left(\frac{G_{los}}{\ell^2}+\frac{G_{ref}}{\tilde{\ell}^2}-\frac{2\sqrt{G_{los}G_{ref}}}{\ell\tilde{\ell}}\cos\underbrace{\left[\frac{\omega}{c}\left(\tilde{\ell}-\ell\right)\right]}_{\Delta\phi}\right) \tag{3}$$

For simplicity, we assume $G_{los}=1$ throughout the following and use the normalized gain $\rho=\sqrt{G_{ref}/G_{los}}$. This yields

$$P_r(d,\omega;h_{\text{Tx}},h_{\text{Rx}},P_t,\rho)= P_t\left(\frac{c}{2\omega}\right)^2\left(\frac{1}{\ell^2}+\frac{\rho^2}{\tilde{\ell}^2}-\frac{2\rho}{\ell\tilde{\ell}}\cos\underbrace{\left[\frac{\omega}{c}\left(\tilde{\ell}-\ell\right)\right]}_{\Delta\phi}\right).$$

Additionally, we assume that the gain on the reflected path is less than on the direct path, i.e., $\rho\leq 1$, e.g., due to additional absorption on the ground.

It is well-known that the two components can interfere constructively or destructively at the receiver, depending on the distance d. This leads to local minima in the receive power at certain distances, which in turn can lead to outages in the transmission. In order to mitigate these drops in the receive power, we propose to use a second frequency in parallel. The exact problem formulation is described in the following.

A. Problem Formulation

Throughout the following, we will consider a two-ray ground reflection scenario where the height of the transmitter h_{Tx}, the height of the receiver h_{Rx}, and the base frequency ω_1 are fixed. In contrast, the distance between transmitter and receiver d varies and is unknown. Only the range of possible distances d is known, i.e., $d\in[d_{\min},d_{\max}]$.

In order to ensure a high reception quality at any distance within the interval, the transmitter employs a second frequency $\omega_2=\omega_1+\Delta\omega$ such that we can compensate for possible destructive interference of the two rays. This leads to the following problem.

Problem Statement 1. Since the transmitter only knows the range of d, i.e., that $d\in[d_{\min},d_{\max}]$, we adjust the frequency spacing $\Delta\omega$ such that the *worst-case* receive power in $[d_{\min},d_{\max}]$ is maximized. This optimization problem can be formulated as

$$\max_{\Delta\omega}\min_{d\in[d_{\min},d_{\max}]}P_{r,1}(d,\omega_1)+P_{r,2}(d,\omega_2), \tag{4}$$

where $P_{r,1}(d,\omega_1)$ is the received power on the first frequency $f_1=\omega_1/(2\pi)$ at distance d and $P_{r,2}(d,\omega_2)$ is the received power for the second frequency $f_2=\omega_2/(2\pi)=(\omega_1+\Delta\omega)/(2\pi)$ at distance d.

III. Single Frequency

In order to solve (4), we first need to analyze the receive power for a single frequency ω. Since we are interested in a worst-case design, we analyze the worst-case receive power of a single frequency in the following. In order to do this, we start by investigating the distances at which destructive interference occurs.

A. Destructive Interference

From (3), it can be seen that we get a (local) minimum of the receive power when the direct and reflected signals interfere destructively [27]. This occurs whenever the phase difference $\Delta\phi$ is a multiple of 2π, i.e.,

$$\Delta\phi=\frac{\omega}{c}\left(\tilde{\ell}-\ell\right)=2\pi k,\quad k\in\mathbb{N}_0. \tag{5}$$

It can easily be verified that $\Delta\phi$ is a decreasing function in d and it therefore follows that

$$\begin{aligned}\Delta\phi_{\max}&=\lim_{d\to 0}\Delta\phi\\&=\frac{2\omega\min\{h_{\text{Tx}},h_{\text{Rx}}\}}{c}\end{aligned}$$

and

$$\lim_{d\to\infty}\Delta\phi=0.$$

This shows that $\Delta\phi$ decreases from a finite value $\Delta\phi_{\max}$ to 0. Hence, there always exists a finite number of multiples of 2π with $k_{\max}=\lfloor\frac{\Delta\phi_{\max}}{2\pi}\rfloor$, i.e., there exist $k_{\max}$ local minima of the receive power.

The distance d_k at which the k-th minimum occurs, is given by solving (5) as

$$d_k^2(\omega)=\frac{\left((c\pi k)^2-(\omega h_{\text{Rx}})^2\right)\left((c\pi k)^2-(\omega h_{\text{Tx}})^2\right)}{(\omega c\pi k)^2}, \tag{6}$$

with $k=1,\ldots,k_{\max}$.

Example 1. An illustration of $\Delta\phi$ can be found in Fig. 2. The parameters are set to $\omega/c=10$ ($f=477\,\text{MHz}$), $h_{\text{Tx}}=10\,\text{m}$, and $h_{\text{Rx}}=1.5\,\text{m}$. Additionally, we indicate the distances d_k. Since $k_{\max}=4$, there exist four d_k at which a local minimum occurs. For the selected parameters, they are evaluated to $d_1=46.7\,\text{m}$, $d_2=21.6\,\text{m}$, $d_3=12.3\,\text{m}$, and $d_4=6.5\,\text{m}$. The corresponding received power from (3) is shown in Fig. 3. It can be seen that a minimum occurs at $d=d_k$, with the lowest minimum being at the smallest k, i.e., $k=1$, which corresponds to the highest distance of all d_k. For comparison, we additionally show the received power for $f_2=2.4\,\text{GHz}$ in Fig. 3.

B. Worst-Case Receive Power

When d is anywhere in the interval $[d_{\min},d_{\max}]$, the lowest drop is at the smallest k such that d_k is still in $[d_{\min},d_{\max}]$. However, in order to determine the global minimum of the receive power in $[d_{\min},d_{\max}]$, the boundary points $d_{\min}$ and $d_{\max}$ need to be taken into account. This leads to the following result of the minimal receive power when only a single frequency is used.

Theorem 1 (Minimal Receive Power (Single Frequency))**.** *Consider the described two-ray ground reflection model with a*

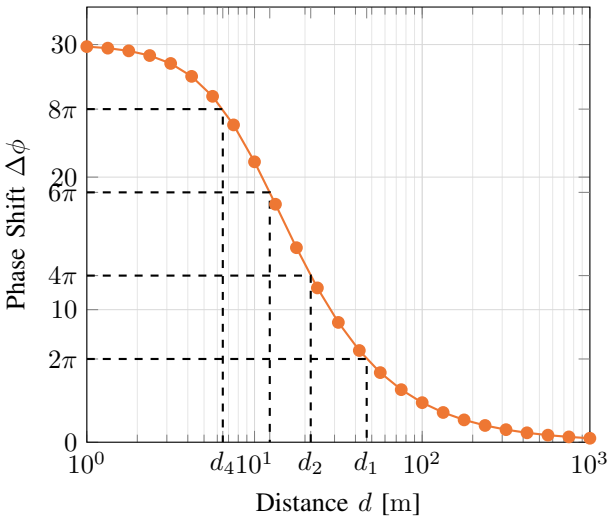


Figure 2. Relative phase shift $\Delta\phi$ from (5) for $\omega/c = 10$, $h_{\text{Tx}} = 10\,\text{m}$, and $h_{\text{Rx}} = 1.5\,\text{m}$. Additionally the distances d_k, $k = 1, \ldots, 4$, from (6) are indicated. (Example 1)

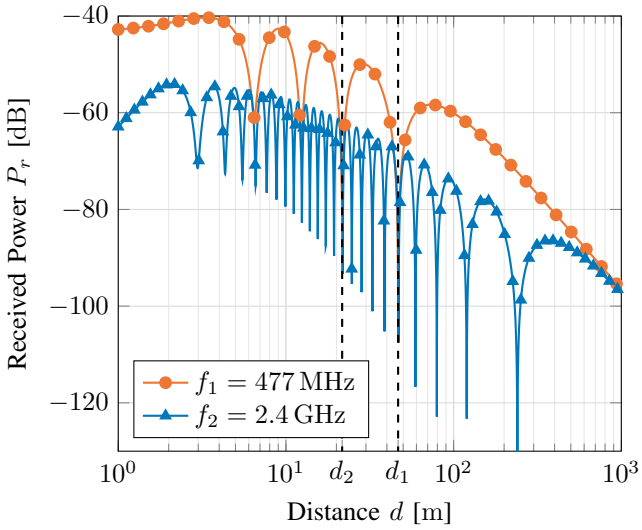


Figure 3. Received power $P_r(d)$ from (3) when using a single frequency f with system parameters $h_{\text{Tx}} = 10\,\text{m}$, $h_{\text{Rx}} = 1.5\,\text{m}$, $\rho = 1$, and $P_t = 1$ for $f = f_1 = 477\,\text{MHz}$ and $f = f_2 = 2.4\,\text{GHz}$. Additionally, the distances $d_1(\omega_1) = 46.7\,\text{m}$ and $d_2(\omega_1) = 21.6\,\text{m}$ from (6) are indicated. (Examples 1 and 2)

single frequency $\omega = 2\pi f$. The distance d between transmitter and receiver is in the interval $[d_{min}, d_{max}]$. The minimal receive power is then given as

$$\min_{d\in[d_{min},d_{max}]} P_r(d) = \min\left\{P_r(d_{min}), P_r(d_{max}), P_r\left(\max_{d_k\in[d_{min},d_{max}]} d_k\right)\right\}. \quad (7)$$

Example 2 (Single Frequency Worst-Case Receive Power). For a numerical example, we take the parameters that are used in Example 1 and additionally compare it to a higher frequency scenario. In particular, we fix $h_{\text{Tx}} = 10\,\text{m}$, $h_{\text{Rx}} = 1.5\,\text{m}$, and $P_t = 1$. We assume a perfect reflection on the ground without any additional absorption, i.e., $\rho = 1$. The receiver is assumed to be randomly located at a distance between $d_{\text{min}} = 30\,\text{m}$ and $d_{\text{max}} = 100\,\text{m}$ from the transmitter.

For the lower frequency $\omega_1 = 10c$, i.e., $f_1 = 477\,\text{MHz}$, we get $P_r(d_{\text{min}}, \omega_1) = -50\,\text{dB}$, $P_r(d_{\text{max}}, \omega_1) = -60\,\text{dB}$, and $P_r(d_1(\omega_1), \omega_1) = -97\,\text{dB}$ with $d_1(\omega_1) = 46.7\,\text{m}$. Based on (7) from Theorem 1, we determine that the worst-case receive power is equal to $-97\,\text{dB}$.

In contrast, for a higher frequency $f_2 = 2.4\,\text{GHz}$, there are multiple local minima at locations d_k, which lie in the interval $[d_{\text{min}}, d_{\text{max}}]$. According to (7), we need to determine the maximum of all $d_k \in [d_{\text{min}}, d_{\text{max}}]$. For the considered parameters, this is calculated to $d_3(\omega_2) = 79.4\,\text{m}$ with $P_r(d_3(\omega_2), \omega_2) = -125\,\text{dB}$. The received powers at the boundary points are evaluated to $P_r(d_{\text{min}}, \omega_2) = -64\,\text{dB}$ and $P_r(d_{\text{max}}, \omega_2) = -75\,\text{dB}$. Hence, the worst-case receive power when using only frequency f_2 is $-125\,\text{dB}$.

Example 3 (Single Frequency Receive Power with Different Gains). In the previous example, we assumed that the antenna and reflection gain on the reflected path is the same as the one on the LoS path, i.e., $\rho = 1$. In practical systems, it is likely that $\rho < 1$, e.g., due to an additional absorption at the ground. Therefore, we compare the receive power for different values of ρ in Fig. 4. The system parameters are again set to $f = 2.4\,\text{GHz}$, $h_{\text{Tx}} = 10\,\text{m}$, $h_{\text{Rx}} = 1.5\,\text{m}$, $P_t = 1$, $d_{\text{min}} = 30\,\text{m}$, and $d_{\text{max}} = 100\,\text{m}$.

For small ρ, the influence of the reflected ray reduces and the total receive power is approximately determined by the path-loss of the LoS component. In this case, the destructive interference only has a negligible effect. For $\rho = 0.1$, the receive power at d_3 is around $-79\,\text{dB}$. At the boundaries of the distance interval, we get $P_r(d_{\text{min}}) = -69.2\,\text{dB}$ and $P_r(d_{\text{max}}) = -79.4\,\text{dB}$. Thus, the worst-case receive power in $[d_{\text{min}}, d_{\text{max}}]$ is given by $P_r(d_{\text{max}})$.

In contrast, for a larger value of $\rho = 0.5$, the destructive interference is significant and we evaluate the receive power at d_3 to $-84.1\,\text{dB}$. This is also the worst-case receive power in the interval $[d_{\text{min}}, d_{\text{max}}]$ for $\rho = 0.5$. Similarly, the worst-case receive power for $\rho = 1$ is also given by the local minimum at d_3 with $P_r(d_3) = -125\,\text{dB}$, cf. Example 2.

It should also be noted that the constructive interference is more significant for large values of ρ. However, since we are interested in ultra-reliable communications, we only focus on the worst-case.

Proposition 1 (Worst-Case ρ)**.** *In general, the destructive interference is getting worse for increasing ρ and attains a minimum at $\rho = \tilde{\ell}/\ell > 1$. However, since we restrict the range of ρ to $0 \le \rho \le 1$, the worst-case interference of the two rays occurs at $\rho = 1$.*

IV. Two Frequencies

Since the drops in receive power due to destructive interference of the two rays cannot be avoided without knowledge of d when a single frequency is used, we will now employ a second frequency to mitigate these minima. As described in Problem Statement 1, we aim to optimize the frequency spacing Δf for a

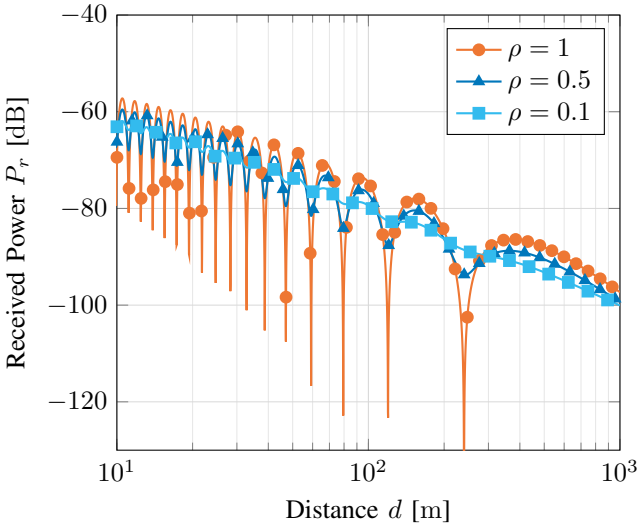


Figure 4. Received power $P_r(d)$ from (3) when using a single frequency $f = 2.4\,\text{GHz}$ with system parameters $h_{\text{Tx}} = 10\,\text{m}$, $h_{\text{Rx}} = 1.5\,\text{m}$, and $P_t = 1$ for different values of ρ. (Example 3)

second frequency $f_2 = f_1 + \Delta f = \omega_2/(2\pi) = (\omega_1 + \Delta\omega)/(2\pi)$ given a base frequency $f_1 = \omega_1/(2\pi)$.

As discussed in Proposition 1, the destructive interference is worst for $\rho = 1$. Therefore, we will only consider this case throughout this section.

The received power at distance d is given as the sum power $P_{r,1}(d, \omega_1) + P_{r,2}(d, \omega_2)$. For a fair comparison with the single frequency case, we assume that the total transmit power P_t remains the same. Thus, for the first frequency, θP_t with $\theta \in [0, 1]$, is used as the transmit power and $\bar{\theta} P_t$, $\bar{\theta} = 1 - \theta$, for the second. This leads to the expression of the total received power in (8) at the bottom of this page.

Since we are particularly interested in improving the worst-case performance, we will consider a lower bound on P_r in the following.

Lemma 1 (Lower Bound on the Sum Power for Two Frequencies)**.** *For the described two-ray ground reflection system using two frequencies ω_1, ω_2 in parallel, the received (sum) power P_r, is lower bounded by* (9) *at the bottom of this page.*

Proof. The proof can be found in Appendix A. □

Proposition 2 (Optimal Power Split for Two Frequencies)**.** *In general, the optimal power split $\theta^\star$, which maximizes P_r, depends on all of the parameters ℓ, $\tilde{\ell}$, ω_1, and $\Delta\omega$. Hence, the optimal power split varies with varying distance d. However, for base frequencies ω_1 which are large compared to the frequency spacing $\Delta\omega$, $\theta^\star$ approaches 0.5, independent of d.*

Since we do not assume exact knowledge about d at the transmitter, we cannot adjust the power split θ to be the exact optimum $\theta^\star$. However, in most communication systems, we typically have the case that $\omega_1 \gg \Delta\omega$. Therefore, the approximation of equal power allocation, i.e., $\theta = 0.5$, from Proposition 2 is a reasonable strategy, which we will use throughout the following.

Example 4 (Sum Power Lower Bound). As an example, we show the received (sum) power from (8) and the lower bound from (9) for $f_1 = 2.4\,\text{GHz}$, $\Delta f = 250\,\text{MHz}$, $h_{\text{Tx}} = 10\,\text{m}$, and $h_{\text{Rx}} = 1.5\,\text{m}$ in Fig. 5. It can clearly be seen that the lower bound is the lower envelope of the actual received power. Similar to the case that only a single frequency is used, the received power varies with the distance d and shows both minima and maxima. While the actual received power P_r oscillates at a high frequency over the distance d, the (spatial) frequency of the lower bound $\underline{P_r}$ is determined by the difference in frequencies $\Delta f = \Delta\omega/(2\pi)$.

In the following, we give an approximation for the locations of the local maxima and minima of $\underline{P_r}$ when two frequencies are used in parallel.

Lemma 2. *For $\omega_1 \gg \Delta\omega$, the bound on the received power $\underline{P_r}$ from* (9) *has a (local) maximum approximately at*

$$\Delta\omega_{\pi,k} = \frac{\pi c}{\tilde{\ell} - \ell}(2k + 1), \quad k \in \mathbb{N}_0\,, \tag{10}$$

and a (local) minimum approximately at

$$\widetilde{\Delta\omega_k} = \frac{2\pi c}{\tilde{\ell} - \ell} k, \quad k \in \mathbb{N}_0\,. \tag{11}$$

Proof. For $\omega_1 \gg \Delta\omega$, we can use the approximation that $\omega_1 \approx \omega_2 = \omega_1 + \Delta\omega$. With this, $\underline{P_r}$ from (9) can be simplified to

$$\underline{P_r} \approx \frac{P_t}{\omega_1^2}\left(\frac{c}{2}\right)^2 \left[\left(\frac{1}{\ell^2} + \frac{1}{\tilde{\ell}^2}\right) - \frac{2}{\ell\tilde{\ell}}\left|\cos\frac{\Delta\phi}{2}\right|\right]$$

with $\Delta\phi = \frac{\Delta\omega}{c}(\tilde{\ell} - \ell)$. From this, it can directly be seen that $\underline{P_r}$ has a local maximum at $\Delta\phi/2 = (2k+1)\pi/2$ and a local minimum at $\Delta\phi/2 = k\pi$ with $k \in \mathbb{N}_0$. Solving this for $\Delta\omega$, we obtain $\Delta\omega_\pi$ and $\widetilde{\Delta\omega}$ from (10) and (11), respectively. □

$$P_r = P_t\left(\frac{c}{2}\right)^2 \left[\left(\frac{\theta}{\omega_1^2} + \frac{\bar{\theta}}{\omega_2^2}\right)\left(\frac{1}{\ell^2} + \frac{1}{\tilde{\ell}^2}\right) - \frac{2}{\ell\tilde{\ell}}\left(\frac{\theta\cos\left(\frac{\omega_1}{c}(\tilde{\ell} - \ell)\right)}{\omega_1^2} + \frac{\bar{\theta}\cos\left(\frac{\omega_2}{c}(\tilde{\ell} - \ell)\right)}{\omega_2^2}\right)\right] \tag{8}$$

$$\underline{P_r}(d, \Delta\omega; \omega_1, h_{\text{Tx}}, h_{\text{Rx}}, P_t, \theta) = P_t\left(\frac{c}{2}\right)^2 \left[\left(\frac{\theta}{\omega_1^2} + \frac{\bar{\theta}}{\omega_2^2}\right)\left(\frac{1}{\ell^2} + \frac{1}{\tilde{\ell}^2}\right) - \frac{2}{\ell\tilde{\ell}}\sqrt{\left(\frac{\theta}{\omega_1^2}\right)^2 + \left(\frac{\bar{\theta}}{\omega_2^2}\right)^2 + \frac{2\theta\bar{\theta}\cos\left(\frac{\Delta\omega}{c}(\tilde{\ell} - \ell)\right)}{\omega_1^2\omega_2^2}}\right] \tag{9}$$

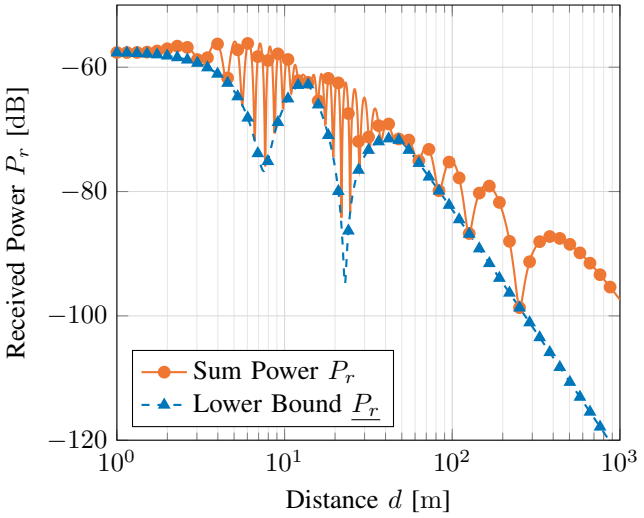


Figure 5. Received power for two parallel frequencies with $f_1 = 2.4\,\text{GHz}$, $\Delta f = 250\,\text{MHz}$, $h_{\text{Tx}} = 10\,\text{m}$, and $h_{\text{Rx}} = 1.5\,\text{m}$. Both the actual value P_r from (8) and the lower bound $\underline{P_r}$ from (9) are shown. (Example 4)

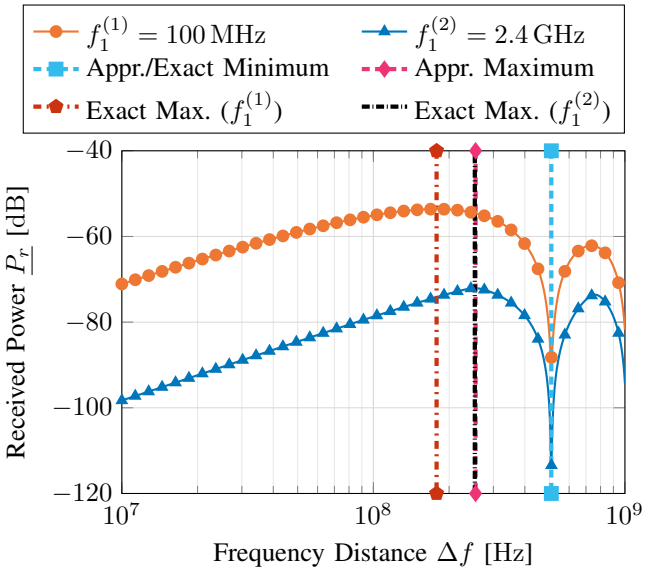


Figure 6. Received power envelope $\underline{P_r}$ for two parallel frequencies f_1 and $f_2 = f_1 + \Delta f$. The additional parameters are set to $d = 50\,\text{m}$, $h_{\text{Tx}} = 10\,\text{m}$, and $h_{\text{Rx}} = 1.5\,\text{m}$. The first peaks are indicated, both the exact locations (numerically determined) and the approximations from Lemma 2. (Example 5)

Remark 1. The important consequence of Lemma 2 is that for large ω_1, $\underline{P_r}(d, \Delta\omega)$ is an increasing function in $\Delta\omega$ for $\widetilde{\Delta\omega_{k-1}} < \Delta\omega < \Delta\omega_{\pi,k}$ and decreasing for $\Delta\omega_{\pi,k} < \Delta\omega < \widetilde{\Delta\omega_k}$, with $k = 1, 2, \ldots$. Also note that we always have $\widetilde{\Delta\omega_0} = 0$, i.e., there is a local minimum at $\Delta\omega = 0$, which corresponds to the single frequency case.

Throughout the following, we will refer to $\Delta\omega_{\pi,1}$ and $\widetilde{\Delta\omega_1}$ from (10) and (11) as simply $\Delta\omega_\pi$ and $\widetilde{\Delta\omega}$, respectively.

Example 5 (Approximation of the Peak Positions). A numerical illustration of the approximations from Lemma 2 can be found in Fig. 6. For the example, we consider two different base frequencies f_1, namely $f_1^{(1)} = 100\,\text{MHz}$ and $f_1^{(2)} = 2.4\,\text{GHz}$. The remaining parameters are fixed to $d = 50\,\text{m}$, $h_{\text{Tx}} = 10\,\text{m}$, and $h_{\text{Rx}} = 1.5\,\text{m}$. Besides the lower bound on the power $\underline{P_r}$ from (9), we show the locations of the first peak $\Delta\omega_\pi$ and drop $\widetilde{\Delta\omega}$. The approximated values are given by (10) and (11) in Lemma 2. For comparison, we additionally indicate the values of the exact minimum and maximum locations, which are determined numerically [24]. First, it can clearly be seen that the approximation of the minimum location $\widetilde{\Delta\omega}$ is very close to the exact value for both base frequencies f_1. Both the approximation and the exact values are evaluated to around $\widetilde{\Delta f} = \widetilde{\Delta\omega}/(2\pi) = 510\,\text{MHz}$.

In contrast, the approximation of the location of the first maximum $\Delta\omega_\pi$ becomes more accurate for large f_1. For the considered parameter values, the approximation from (10) is evaluated to $\Delta f_\pi = \Delta\omega_\pi/(2\pi) = 255\,\text{MHz}$. For $f_1^{(1)}$, the maximum actually occurs at around $\Delta f = 178\,\text{MHz}$, which corresponds to a relative error of around $43\,\%$. However, for the larger base frequency $f_1^{(2)}$, the exact location of the maximum is at around $253\,\text{MHz}$. In this case, the relative error of the approximation is only around $0.79\,\%$. This indicates that the approximation is accurate enough for practical purposes when considering typical base frequencies of above $2\,\text{GHz}$.

As can be seen from the example above, when using two frequencies ω_1 and $\omega_2 = \omega_1 + \Delta\omega$, the receive power can be varied for a given distance d by adjusting $\Delta\omega$. This directly leads to the following optimization of $\Delta\omega$.

A. Optimal Frequency Spacing

Recall from Problem Statement 1 that we are interested in the optimization problem

$$\max_{\Delta\omega} \min_{d\in[d_{\min}, d_{\max}]} \underline{P_r}(d, \Delta\omega)\,, \tag{12}$$

where $d_{\min}$ and $d_{\max}$ denote the known interval boundaries of the distance d between transmitter and receiver. In order to solve this optimization problem, we need the following characterization.

Lemma 3. *The optimization problem from* (12) *can be reformulated as*

$$\max_{\Delta\omega\in[0,\widetilde{\Delta\omega}(d_{max})]} \min\left\{\underline{P_r}(d_{max}, \Delta\omega), g(\Delta\omega)\right\}\,. \tag{13}$$

with

$$g(\Delta\omega) = \begin{cases} \underline{P_r}(d_{min}, \Delta\omega) & \text{if} \quad 0 < \Delta\omega < \widetilde{\Delta\omega}(d_{min}) \\ \underline{P_r}(d_1, \Delta\omega) & \text{if} \quad \widetilde{\Delta\omega}(d_{min}) \le \Delta\omega < \widetilde{\Delta\omega}(d_{max}) \end{cases} \tag{14}$$

and $\underline{P_r}(d_1, \Delta\omega)$ *in* (15) *at the top of the next page.*

Proof. The proof can be found in Appendix B. □

Based on the reformulation of the original optimization problem, we can determine the optimal frequency spacing $\Delta\omega$ for worst-case design as follows.

Theorem 2 (Optimal Frequency Spacing for Worst-Case Design)**.** *Consider the described communication system, where two frequencies* ω_1 *and* $\omega_2 = \omega_1 + \Delta\omega$ *are used in parallel.*

$$\underline{P_r}(d_1, \Delta\omega) = \frac{P_t}{2}\left(\frac{c^2\pi\Delta\omega}{2}\right)^2\left(\frac{1}{\omega_1^2}+\frac{1}{\omega_2^2}\right)\left(\frac{1}{\sqrt{(c^2\pi^2 - h_{\mathrm{Rx}}h_{\mathrm{Tx}}\Delta\omega^2)^2}} - \frac{1}{\sqrt{(c^2\pi^2 + h_{\mathrm{Rx}}h_{\mathrm{Tx}}\Delta\omega^2)^2}}\right)^2 \tag{15}$$

The optimal frequency spacing for worst-case design $\Delta\omega^\star$ is given by the intersection of $\underline{P_r}(d_{max}, \Delta\omega)$ and $g(\Delta\omega)$ from (14) in the interval $\Delta\omega \in [\Delta\omega_\pi(d_{min}), \Delta\omega_\pi(d_{max})]$, if it exists. Otherwise, if no intersection exists, it is given by the maximum of $\underline{P_r}(d_{max}, \Delta\omega)$, which is approximately located at

$$\Delta\omega^\star \approx \frac{c\pi}{\tilde{\ell}(d_{max}) - \ell(d_{max})} = \Delta\omega_\pi(d_{max})\,. \tag{16}$$

Proof. The proof can be found in Appendix C. □

Based on Theorem 2, we can summarize the steps to calculate the optimal frequency spacing $\Delta f^\star = \omega^\star/(2\pi)$ for a worst-case design with given model parameters in Algorithm 1. The function `FindIntersection` in Lines 9 and 12 could be any routine that allows calculating the intersection between an increasing and a decreasing function, e.g., by minimizing the (quadratic) distance between them. A Python implementation with interactive notebooks to reproduce all of the calculations can be found at [24].

Example 6 (Optimal Frequency Spacing for Worst-Case Design). As an illustration, we evaluate the following numerical example in detail. As a base frequency, we choose $f_1 = 2.4\,\mathrm{GHz}$. The transmitter is located at height $h_{\mathrm{Tx}} = 10\,\mathrm{m}$ and the receiver at $h_{\mathrm{Rx}} = 1.5\,\mathrm{m}$. While the distribution of the distance between transmitter and receiver is unknown, it is known that the receiver can only be located at a distance between $d_{\min} = 10\,\mathrm{m}$ and $d_{\max} = 100\,\mathrm{m}$. The optimal frequency gap Δf will therefore lie below $\widetilde{\Delta f}(d_{\max}) = 1\,\mathrm{GHz}$. In Fig. 7, we show $\underline{P_r}(d_{\min}, \Delta\omega)$, $\underline{P_r}(d_1, \Delta\omega)$, and $\underline{P_r}(d_{\max}, \Delta\omega)$ over the frequency spacing $\Delta f = \Delta\omega/(2\pi)$. First, it can be seen that both $\underline{P_r}(d_{\min})$ and $\underline{P_r}(d_1)$ are decreasing. Recall that these functions define the function g from (14). On the other hand, $\underline{P_r}(d_{\max})$ increases for $\Delta\omega < \Delta\omega_\pi(d_{\max}) = 502\,\mathrm{MHz}$. Next, there exists exactly one intersection of $\underline{P_r}(d_{\max})$ and g at around $\Delta f = 177\,\mathrm{MHz}$. According to Theorem 2, this corresponds to the optimal frequency spacing $\Delta f^\star$ that maximizes the worst-case receive power. The corresponding worst-case power is calculated to $-85.7\,\mathrm{dB}$.

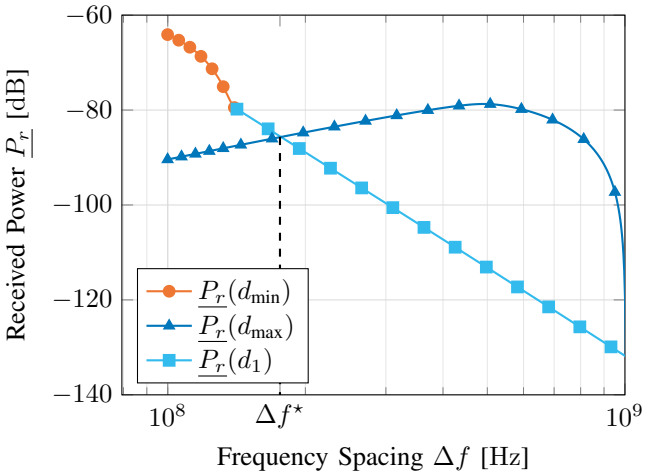


Figure 7. Receive powers $\underline{P_r}(d_{\min})$, $\underline{P_r}(d_1)$, and $\underline{P_r}(d_{\max})$ over the frequency spacing Δf for system parameters $f_1 = 2.4\,\mathrm{GHz}$, $h_{\mathrm{Tx}} = 10\,\mathrm{m}$, $h_{\mathrm{Rx}} = 1.5\,\mathrm{m}$, $d_{\min} = 10\,\mathrm{m}$, and $d_{\max} = 100\,\mathrm{m}$. The optimal frequency spacing $\Delta f^\star$, i.e., the maximum of the minimum of the curves, can be found at around $\Delta f^\star = 177\,\mathrm{MHz}$. (Example 6)

Algorithm 1 Procedure to Find the Optimal Frequency Spacing $\Delta\omega^\star$ for Worst-Case Design

1: **function** OPTIMALFREQUENCYSPACING(f_1, $d_{\min}$, $d_{\max}$, h_{Tx}, h_{Rx})
2: Calculate $\Delta\omega_\pi(d_{\min})$ and $\Delta\omega_\pi(d_{\max})$ // According to (10)
3: Calculate $\widetilde{\Delta\omega}(d_{\min})$ and $\widetilde{\Delta\omega}(d_{\max})$ // According to (11)
4: **if** $\underline{P_r}(d_{\max}, \Delta\omega_\pi(d_{\max}) < g(\Delta\omega_\pi(d_{\max}))$ **then** // No intersection
5: $\Delta\omega^\star = \Delta\omega_\pi(d_{\max})$ // According to (16)
6: **else** // An intersection between $\underline{P_r}$ and g exists
7: **if** $\underline{P_r}(d_{\max}, \widetilde{\Delta\omega}(d_{\min}) > \underline{P_r}(d_{\min}, \widetilde{\Delta\omega}(d_{\min}))$ **then**
8: // Intersection in $[\Delta\omega_\pi(d_{\min}), \widetilde{\Delta\omega}(d_{\min})]$
9: $\Delta\omega^\star = $ FINDINTERSECTION($\underline{P_r}(d_{\min}, \Delta\omega)$, $\underline{P_r}(d_{\max}, \Delta\omega)$) for $\Delta\omega_\pi(d_{\min}) < \Delta\omega < \widetilde{\Delta\omega}(d_{\min})$
10: **else**
11: // Intersection in $[\widetilde{\Delta\omega}(d_{\min}), \widetilde{\Delta\omega}(d_{\max})]$
12: $\Delta\omega^\star = $ FINDINTERSECTION($\underline{P_r}(d_1, \Delta\omega)$, $\underline{P_r}(d_{\max}, \Delta\omega)$) for $\widetilde{\Delta\omega}(d_{\min}) < \Delta\omega < \widetilde{\Delta\omega}(d_{\max})$
13: **end if**
14: **end if**
15: $\Delta f^\star = \Delta\omega^\star/(2\pi)$
16: **return** $\Delta f^\star$
17: **end function**

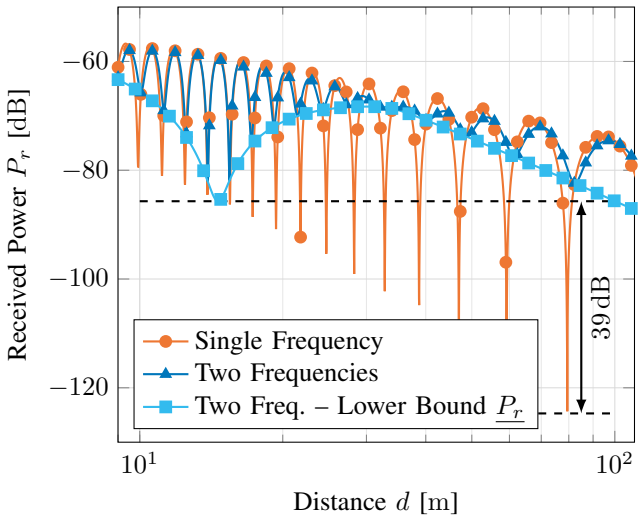


Figure 8. Received powers for a two-ray ground reflection scenario with parameters $f_1 = 2.4\,\text{GHz}$, $h_{\text{Tx}} = 10\,\text{m}$, $h_{\text{Rx}} = 1.5\,\text{m}$, $d_{\text{min}} = 10\,\text{m}$, and $d_{\text{max}} = 100\,\text{m}$. First, the receiver power for a single frequency with $f = f_1$ from (3) is shown. Additionally, the received power for two parallel frequencies with $\Delta f = \Delta f^\star = 177\,\text{MHz}$ from (8) and its lower bound from (9) are depicted. (Example 6)

A comparison with the single frequency case is shown in Fig. 8. Besides the single frequency case, the actual received power and its lower bound are depicted for the scenario that two frequencies are used in parallel with optimal frequency spacing $\Delta f = \Delta f^\star$. When only a single frequency is used, there exist multiple local minima in $[d_{\text{min}}, d_{\text{max}}]$ with a decreasing receive power. The global minimum in $[d_{\text{min}}, d_{\text{max}}]$ for the above parameters can be calculated according to Theorem 1 to around $-124.7\,\text{dB}$ at the distance of around $79.4\,\text{m}$. In contrast, the received power with two parallel frequencies is always greater than $-85.7\,\text{dB}$. Thus, by using a second frequency, the worst-case receive power is improved by around $39\,\text{dB}$.

V. Achievable Rate Analysis

After investigating the receive power, we now take a closer look at the resulting achievable data rate. For a single frequency band of bandwidth B around the carrier frequency $\omega_1 = 2\pi f_1$, the capacity is in general given as [28, Chap. 5]

$$R_1 = \int_{f_1 - B/2}^{f_1 + B/2} \log_2 \left(1 + \frac{P_r(f; P_t/B)}{F N_0} \right) \mathrm{d}f \,, \tag{17}$$

where $P_r(f; P_t/B)$ is the receive power at frequency f and the transmit power is assumed to be equally distributed over the bandwidth B. Furthermore, N_0 is the noise spectral density and F the receiver noise figure.

However, this expression can be simplified for small bandwidths compared to the carrier frequency. With this narrowband assumption, the capacity can be calculated as [28, Chap. 5]

$$R_1 = B \log_2 \left(1 + \frac{P_r(\omega_1; P_t)}{B F N_0} \right) , \tag{18}$$

where $P_r(\omega_1; P_t)$ denotes the receive power from (3) with transmit power P_t.

For a fair comparison, the bandwidth is split into two separate frequency bands of size $B/2$ in the case of two parallel frequencies. This yields the total (sum) rate

$$R_2 = \frac{B}{2} \log_2 \left(1 + \frac{P_{r,1}(\omega_1; P_t/2)}{F N_0 \frac{B}{2}} \right) + \frac{B}{2} \log_2 \left(1 + \frac{P_{r,2}(\omega_2; P_t/2)}{F N_0 \frac{B}{2}} \right) , \tag{19}$$

where $P_{r,i}(\omega_i)$ again denotes the receive power on frequency ω_i.

As before, it should be emphasized that the transmit power is kept constant. Hence, it is split in the case of two parallel frequencies. We again assume an equal power split, i.e., $\theta = 0.5$.

In Section IV, we optimized the frequency spacing $\Delta\omega$ such that the worst-case (sum) receive power is maximized. With the following lemma, we show that this result can also be used for worst-case design in terms of the achievable rate.

Lemma 4. *Considering the described communication system, where two frequencies ω_1 and $\omega_2 = \omega_1 + \Delta\omega$ are used in parallel. The lower bound on the achievable rate R_2 is maximized by optimal frequency spacing $\Delta\omega^\star$ from Theorem 2. The worst-case achievable rate $\underline{R_2}$ in the distance interval $[d_{min}, d_{max}]$ is then given by*

$$R_2 \geq \underline{R_2} = \frac{B}{2} \log_2 \left(1 + \alpha + \frac{\underline{P_r}(d, \Delta\omega^\star)}{F N_0 \frac{B}{2}} \right) , \tag{20}$$

where $\underline{P_r}$ is the lower bound on the sum receive power from (9) *and the offset α is given by*

$$\alpha = \left(\frac{1}{F N_0 \frac{B}{2}} \right)^2 \left(\frac{P_t}{2\omega_1 \omega_2} \right)^2 \left(\frac{c}{2} \right)^4 \left(\frac{1}{\ell} - \frac{1}{\bar{\ell}} \right)^4 \Bigg|_{d = d_{max}} . \tag{21}$$

Proof. The proof can be found in Appendix D. □

Example 7 (Achievable Rate Comparison). In order to illustrate the benefit of using two frequencies in terms of achievable rate, we consider the following numerical example. We assume the same system parameters as in Example 6, i.e., $f_1 = 2.4\,\text{GHz}$, $h_{\text{Tx}} = 10\,\text{m}$, $h_{\text{Rx}} = 1.5\,\text{m}$, $d_{\text{min}} = 10\,\text{m}$, and $d_{\text{max}} = 100\,\text{m}$. Based on Lemma 4, the optimal frequency spacing is again $\Delta f^\star = 177\,\text{MHz}$.

Additionally, we consider a bandwidth of $B = 100\,\text{kHz}$. Recall that the bandwidth is split in the case of two frequencies, such that each frequency band only has a bandwidth of $50\,\text{kHz}$. For the receiver noise, we assume a noise figure of $F = 3\,\text{dB}$ and a noise spectral density of $N_0 = -174\,\text{dBm/Hz}$.

In Figure 9, we show the achievable rates for the single frequency case and the scenario with two frequencies with optimal frequency spacing $\Delta f = \Delta f^\star$. We show both the exact rate R_2 from (19) and the lower bound $\underline{R_2}$ from (20).

First, it can clearly be seen that the data rate drops significantly at certain distances when only a single frequency is used. These distances correspond to the distances d_k at which the receive power drops to a local minimum, cf. Section III.

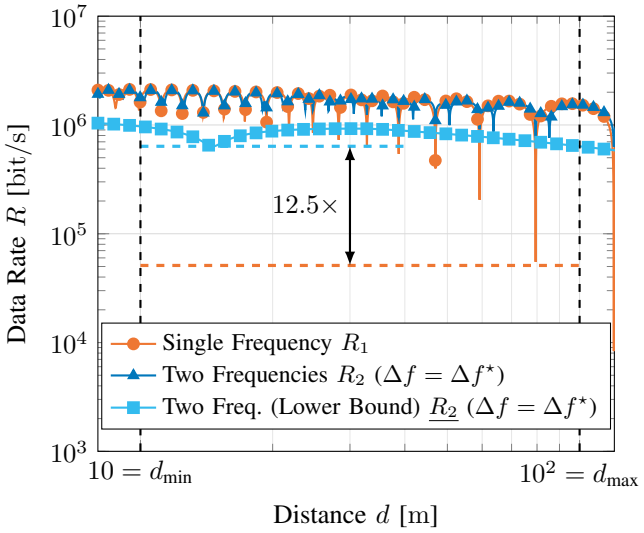


Figure 9. Achievable rates for a two-ray ground reflection scenario with parameters $f_1 = 2.4\,\text{GHz}$, $B = 100\,\text{kHz}$, $h_{\text{Tx}} = 10\,\text{m}$, $h_{\text{Rx}} = 1.5\,\text{m}$, $d_{\text{min}} = 10\,\text{m}$, and $d_{\text{max}} = 100\,\text{m}$. First, the rate R_1 for a single frequency with $f = f_1$ from (18) is shown. Additionally, the achievable rate for two parallel frequencies with $\Delta f = \Delta f^\star = 177\,\text{MHz}$ from (19) and its lower bound from (20) are depicted. (Example 7)

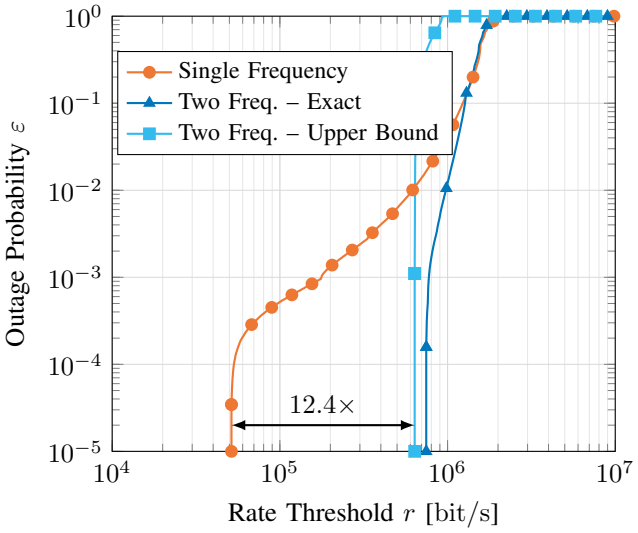


Figure 10. Outage probability for a two-ray ground reflection scenario with $h_{\text{Tx}} = 10\,\text{m}$, $h_{\text{Rx}} = 1.5\,\text{m}$, $f_1 = 2.4\,\text{GHz}$, $\Delta f = 177\,\text{MHz}$, and $B = 100\,\text{kHz}$. The distance d between transmitter and receiver is uniformly distributed between $d_{\text{min}} = 10\,\text{m}$ and $d_{\text{max}} = 100\,\text{m}$, i.e., $d \sim \mathcal{U}[10, 100]\text{m}$. The shown outage probabilities are obtained by MC simulations with 10^7 samples. (Example 8)

For the selected system parameters, the lowest rate of around $51.1\,\text{kbit/s}$ occurs at distance $d = 79.4\,\text{m}$.

In contrast, when employing two frequencies in parallel, the achievable rate is more stable across the distance d. The lowest value of the lower bound $\underline{R_2}$ is evaluated to around $636.8\,\text{kbit/s}$. This amounts to a $12.5\times$ improvement of the worst-case rate compared to the single frequency case. Additionally, it should be noted that $\underline{R_2}$ is only a lower bound on the actual rate R_2, which therefore is even higher.

VI. Outage Probability

As shown in the previous sections, it can be beneficial to use two frequencies in parallel in order to improve the minimum receive power and achievable data rate. This directly translates to improving the reliability of the communication system. Therefore, we analyze the outage probability in the following and show how the proposed scheme enables ultra-reliable communications without perfect CSI at the transmitter.

Throughout the following, we define that an outage occurs when the achievable rate R drops below a threshold r [28]. Thus, the outage probability ε is given as

$$\varepsilon = \Pr\left(R < r\right) . \tag{22}$$

When replacing the actual rate R by the lower bound $\underline{R}$, we obtain an upper bound $\overline{\varepsilon}$ on the actual outage probability, i.e., a worst-case bound.

In the following, we assume a random distribution of the distance d over the interval $[d_{\text{min}}, d_{\text{max}}]$. Based on this, we can express the outage probability as

$$\varepsilon = \int_{R(d)<r} p_d(d)\mathrm{d}d \tag{23}$$

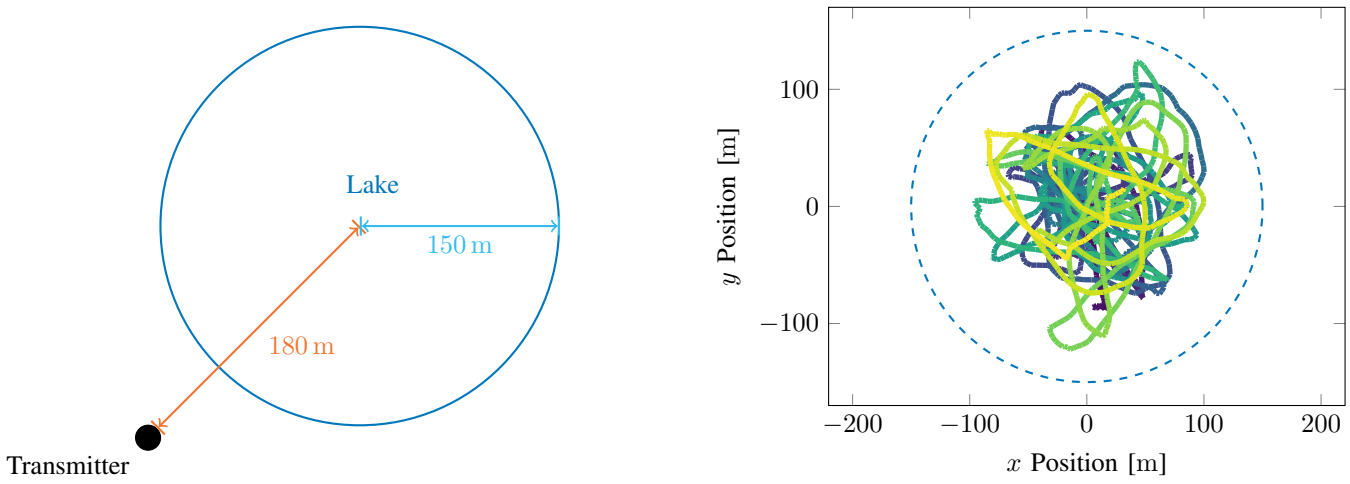
where p_d denotes the PDF of d.

Since the integral in (23) does not admit a closed-form solution for most common distributions of d, we will resort to Monte Carlo (MC) simulations in the following. The source code to reproduce all of the following simulations is available at [24].

Remark 2 (Zero-Outage Capacity). Recall that our considered Problem Statement 1 is to maximize the minimum receive power, and consequently the minimum rate, over a given interval $[d_{\text{min}}, d_{\text{max}}]$ of the distance d. Thus, all achievable rates in the interval are greater than this minimum. Based on this, it can be seen from (22) that the outage probability ε is zero for rate thresholds r less than the minimum achievable rate. Hence, the minimum achievable rate in $[d_{\text{min}}, d_{\text{max}}]$ is also the zero-outage capacity (ZOC) [6], which is defined as the maximum rate, such that the outage probability is zero. The optimization of the frequency spacing Δf presented in this work, therefore, also maximizes the ZOC for a given distance interval $[d_{\text{min}}, d_{\text{max}}]$.

Example 8 (Uniform Distribution of the Distance). As a first numerical example, we consider a uniform distribution of the distance over the interval $[d_{\text{min}}, d_{\text{max}}]$. In this case, we have that $p_d(d) = 1/(d_{\text{max}} - d_{\text{min}})$. While this simplifies the integral in (23), we are still not able to derive a closed-form solution. Thus, the outage probabilities shown in Fig. 10 are obtained by MC simulations with 10^7 samples. The system parameters are again set to the parameters used in Example 7.

The first shown outage probability ε is for the single frequency case, where ε is determined by rate R_1 from (18). It can be seen that there are zero outages below a rate of around $51.1\,\text{kbit/s}$, which corresponds to the worst-case rate over the considered distance interval $[d_{\text{min}}, d_{\text{max}}]$, cf. Example 7. As mentioned in Remark 2, this also corresponds to the ZOC. Above this rate, the outage probability slowly increases. In



(a) Geometrical setup of the UAV example.

(b) Sample trajectory of the UAV with indicated outline of the lake.

Figure 11. Setup of the numerical example of a UAV flying above flat terrain. The movement of the UAV is modeled according to [29] with movement parameters $\alpha_1 = \alpha_2 = 1$, $\beta_1 = \beta_2 = 3$, $\gamma_1 = \gamma_2 = 7$, $\sigma_1 = \sigma_2 = 1$, and $s_1 = s_2 = 1$. (Example 9)

contrast, when using two frequencies in parallel, the increase of the outage probability is much steeper for an increasing rate threshold r. This indicates that the rates are more concentrated at similar values over all distances in the considered interval. This property can also be observed in Fig. 9. It is similar for both the exact outage probability based on R_2 from (19) and the upper bound $\overline{\varepsilon}$ determined by $\underline{R_2}$ from (20). Due to this step-like behavior, the ε-outage capacity for small ε is significantly higher for two frequencies compared to the single frequency case. This includes the ZOC, which is at around $636.8\,\mathrm{kbit/s}$ for the upper bound.

In the context of ultra-reliable communications, we are typically interested in outage probabilities lower than 10^{-5} [3]. In this regard, the advantage of the proposed frequency diversity scheme can clearly be seen.

However, since the assumption of a uniform distribution of the distance in Example 8 seems arbitrary, we now evaluate a more realistic example of a UAV flying above flat terrain.

Example 9 (UAV Flying Above Flat Terrain). The basic simulation scenario is depicted in Fig. 11(a). We consider a flat terrain with a circular lake with a radius of $150\,\mathrm{m}$, which is the area of interest for the UAV deployment. The transmitter is located at a distance of $30\,\mathrm{m}$ from the edge of the lake at height $h_{\mathrm{Tx}} = 10\,\mathrm{m}$. The UAV flies at height $h_{\mathrm{Rx}} = 3\,\mathrm{m}$ above the ground. Its movement is modeled according to the mobility model from [29], which is based on stochastic differential equations (SDEs) for each dimension. For the MC simulation, we fixed the height of the UAV and only considered the movement in x and y direction. The movement parameters are set to $\alpha_1 = \alpha_2 = 1$, $\beta_1 = \beta_2 = 3$, $\gamma_1 = \gamma_2 = 7$, $\sigma_1 = \sigma_2 = 1$, and $s_1 = s_2 = 1$, cf. [29, Sec. II]. A sample trajectory of the UAV based on the SDE model with the described parameters can be found in Fig. 11(b). For the simulation of the outage probability, we generate 1000 trajectories with 2000 positions each, i.e., we obtain a total of $2 \cdot 10^6$ samples. The source code to reproduce all of the presented results can be found at [24].

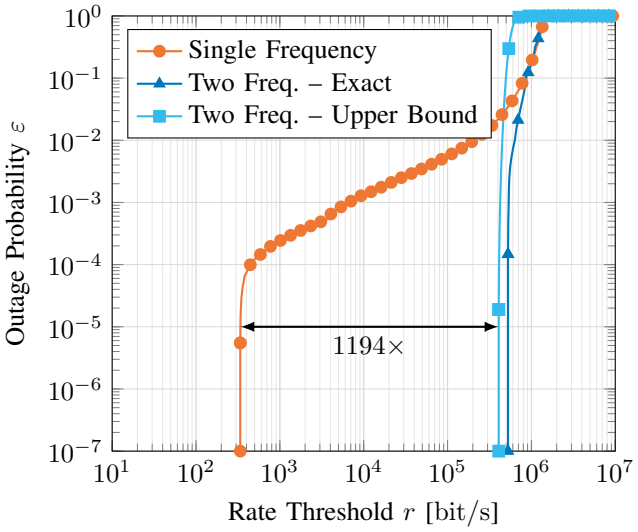


Figure 12. Outage probability for a two-ray ground reflection scenario of a UAV flying above flat terrain. The system parameters are $h_{\mathrm{Tx}} = 10\,\mathrm{m}$, $h_{\mathrm{Rx}} = 3\,\mathrm{m}$, $f_1 = 2.4\,\mathrm{GHz}$, $\Delta f = 190\,\mathrm{MHz}$, and $B = 100\,\mathrm{kHz}$. The distance d between transmitter and receiver is randomly distributed between $d_{\mathrm{min}} = 30\,\mathrm{m}$ and $d_{\mathrm{max}} = 330\,\mathrm{m}$. The shown outage probabilities are obtained by MC simulations with $2 \cdot 10^6$ samples. (Example 9)

The communication system parameters are set to $f_1 = 2.4\,\mathrm{GHz}$, $B = 100\,\mathrm{kHz}$, $F = 3\,\mathrm{dB}$, and $N_0 = -174\,\mathrm{dBm/Hz}$. From the geometrical model, we can derive that the distance d between transmitter and receiver (UAV) is between $d_{\mathrm{min}} = 30\,\mathrm{m}$ and $d_{\mathrm{max}} = 330\,\mathrm{m}$. Based on Theorem 2, the optimal frequency spacing for this setup is $\Delta f = \Delta f^\star = 190\,\mathrm{MHz}$.

The resulting outage probabilities for the single frequency and two frequencies scenario are shown in Fig. 12. Similarly to Example 8, it can be seen that the outage probability for a single frequency decreases slowly when decreasing the rate threshold. In contrast, the achievable rates are more concentrated when using two frequencies in parallel, which results in a steeper outage probability curve in Fig. 12. This results in a higher

ε-outage capacity for small ε. Assuming that the application can tolerate an outage probability of up to $\varepsilon = 10^{-5}$, the rate would have to be adjusted to be less than around $0.339\,\mathrm{kbit/s}$. In contrast, when using two frequencies in parallel with the optimal frequency spacing $\Delta f = \Delta f^\star$, the rate could be up to $404.9\,\mathrm{kbit/s}$, while still fulfilling the same reliability constraint. This corresponds to a gain of nearly $1200\times$ for the ε-outage capacity with $\varepsilon = 10^{-5}$.

This practical example highlights the significant reliability improvements that are possible when using two frequencies in parallel with the optimal frequency spacing. It should also be emphasized that this scheme only requires knowledge of the interval of possible distances between transmitter and receiver *without* requiring perfect CSI at the transmitter.

VII. Conclusion

In this work, we have investigated the receive power, achievable rate, and outage probability in two-ray ground reflection scenarios with unknown distance between transmitter and receiver. We have shown that using two frequencies in parallel can significantly improve the reliability over using only a single frequency. In particular, we derived the optimal frequency spacing such that the worst-case receive power is maximized. An especially useful aspect of the presented results is that only very limited knowledge is required at the transmitter.

All of the results have been evaluated for various numerical examples, including a realistic scenario of a UAV flying above flat terrain. This allows a quantitative classification of the performance improvement by the proposed scheme.

While only two parallel frequencies are considered in this work, it could be extended to a diversity systems with multiple frequencies in future work. This is a promising research direction to further improve the reliability of the described communication systems. Additionally, when adding the assumption that the transmitter has knowledge of the distribution of the distances between transmitter and receiver, the optimization problem could be modified to minimize the outage probability for the given distribution.

Appendix A
Proof of Lemma 1

The lower bound on P_r from (8) is calculated as the (lower) envelope of the function, which is given as the absolute value of its analytic function [30]. However, we are only interested in bounding the oscillating part of P_r given by the cosine terms as

$$s = \frac{\theta \cos\left(\frac{\omega_1}{c}(\tilde{\ell} - \ell)\right)}{\omega_1^2} + \frac{\bar{\theta} \cos\left(\frac{\omega_2}{c}(\tilde{\ell} - \ell)\right)}{\omega_2^2}\,.$$

The analytic function of s is given as $s + \mathrm{j}\hat{s}$, where $\hat{s} = \mathcal{H}\{s\}$ is the Hilbert transform $\mathcal{H}$ of s. The envelope of s is then given as $|s + \mathrm{j}\hat{s}|$. With the correspondence $\mathcal{H}\{\cos(\omega t)\} = \sin(\omega t)$ [31], we obtain the analytic signal

$$s + \mathrm{j}\hat{s} = \frac{\theta \cos(\omega_1 t)}{\omega_1^2} + \frac{\bar{\theta} \cos(\omega_2 t)}{\omega_2^2} + \mathrm{j}\left(\frac{\theta \sin(\omega_1 t)}{\omega_1^2} + \frac{\bar{\theta} \sin(\omega_2 t)}{\omega_2^2}\right),$$

where we use the shorthand $t = \frac{\tilde{\ell} - \ell}{c}$. The absolute value can then be calculated as

$$|s + \mathrm{j}\hat{s}|^2 = \frac{\theta^2}{\omega_1^4} + \frac{\bar{\theta}^2}{\omega_2^4} + \frac{2\theta\bar{\theta}\cos\left((\omega_2 - \omega_1)t\right)}{\omega_1^2\omega_2^2}\,.$$

Applying the definitions of t and $\Delta\omega = \omega_2 - \omega_1$ and substituting the envelope of s into (8), we obtain (9).

Appendix B
Proof of Lemma 3

Similarly to the minimum received power from (7) in the single frequency case, the minimum received power in the two frequency case is given as the minimum over the boundary points and the lowest local minimum peak at distance d_k. As before, the worst case among the d_k is found at d_1. Therefore, if $d_1 \in [d_{\min}, d_{\max}]$, the minimum of $\underline{P_r}$ is given as

$$\min_{d \in [d_{\min}, d_{\max}]} \underline{P_r}(d, \Delta\omega) = \min\left\{\underline{P_r}(d_{\min}, \Delta\omega), \underline{P_r}(d_{\max}, \Delta\omega), \underline{P_r}(d_1, \Delta\omega)\right\},$$

for a given value of $\Delta\omega$.

However, since we can adjust the frequency gap $\Delta\omega$, we can influence the distance d_1 at which the drop in received power occurs. In order to achieve this drop at a given distance d_1, the frequency spacing $\Delta\omega$ needs to be adjusted as $\Delta\omega = \widetilde{\Delta\omega}(d_1)$ based on (11). With this, we obtain $\underline{P_r}(d_1, \Delta\omega)$ according to (15). As mentioned above, in the worst case, we have that $d_1 \in [d_{\min}, d_{\max}]$. In order for this to happen, $\Delta\omega$ needs to be within

$$\widetilde{\Delta\omega}(d_{\min}) \leq \Delta\omega < \widetilde{\Delta\omega}(d_{\max})\,. \tag{24}$$

In this case, it is straightforward to verify that $\underline{P_r}(d_1, \Delta\omega) < \underline{P_r}(d_{\min}, \Delta\omega)$, hence, the minimum receive power is determined as the minimum between $\underline{P_r}(d_1, \Delta\omega)$ and $\underline{P_r}(d_{\max}, \Delta\omega)$.

For $0 < \Delta\omega < \widetilde{\Delta\omega}(d_{\min})$, there is no local minimum in $[d_{\min}, d_{\max}]$ and the minimum receive power is given as the minimum between $\underline{P_r}(d_{\min})$ and $\underline{P_r}(d_{\max})$. Therefore, we introduce the auxiliary function g as

$$g(\Delta\omega) = \begin{cases} \underline{P_r}(d_{\min}, \Delta\omega) & 0 < \Delta\omega < \widetilde{\Delta\omega}(d_{\min}) \\ \underline{P_r}(d_1, \Delta\omega) & \widetilde{\Delta\omega}(d_{\min}) \leq \Delta\omega < \widetilde{\Delta\omega}(d_{\max})\,. \end{cases}$$

Combining all of the above, the optimization problem from (12) can then be rewritten as (13).

Appendix C
Proof of Theorem 2

From Lemma 3, we know that the optimal frequency spacing $\Delta\omega^\star$ is given as the solution to (13). In order to solve (13), we start with the simple observation that $\underline{P_r}$ approaches a finite positive value for $\Delta\omega = 0$, for which additionally $\underline{P_r}(d_{\min}, 0) > \underline{P_r}(d_{\max}, 0)$ holds since $d_{\min} < d_{\max}$.

First, we prove the second part of the theorem, when no intersection between g and $\underline{P_r}(d_{\max})$ exists. Since $\underline{P_r}(d_{\max}) < g$ holds for $\Delta\omega = 0$ and no intersection exists, we have that $\underline{P_r}(d_{\max}) < g$ for the whole domain $0 \leq \Delta\omega < \widetilde{\Delta\omega}(d_{\max})$. Hence, the minimum between $\underline{P_r}(d_{\max})$ and g is simply

$\underline{P_r}(d_{\max})$ and the optimization problem (13) reduces to determining the maximum of $\underline{P_r}(d_{\max})$. By Lemma 2, this can approximately be found at $\Delta\omega^\star = \Delta\omega_\pi$, i.e., (16) from the statement of the theorem.

Next, we consider the case that an intersection between $\underline{P_r}(d_{\max})$ and g exists. It is straightforward to verify that $\underline{P_r}(d_1)$ is strictly decreasing for $\widetilde{\Delta\omega}(d_{\min}) \leq \Delta\omega < \widetilde{\Delta\omega}(d_{\max})$. Based on Lemma 2, we have established that $\underline{P_r}(d_{\min})$ is increasing for $\Delta\omega < \Delta\omega_\pi(d_{\min})$ and decreasing for $\Delta\omega_\pi(d_{\min}) < \Delta\omega < \widetilde{\Delta\omega}(d_{\min})$. Hence, g is increasing for $\Delta\omega < \Delta\omega_\pi(d_{\min})$ and decreasing for $\Delta\omega_\pi(d_{\min}) < \Delta\omega < \widetilde{\Delta\omega}(d_{\max})$. Similarly, we find that $\underline{P_r}(d_{\max})$ is increasing up to $\Delta\omega_\pi(d_{\max})$ and decreasing on the rest of the domain.

From the definitions of ℓ and $\tilde{\ell}$, it can easily be seen that their difference $\tilde{\ell} - \ell$ decreases for an increasing distance d. Thus, it follows that $\Delta\omega_\pi(d_{\max}) > \Delta\omega_\pi(d_{\min})$, i.e., the maximum of $\underline{P_r}(d_{\max})$ occurs at a higher frequency distance $\Delta\omega$ than the maximum of $\underline{P_r}(d_{\min})$. Additionally, it follows from $d_{\max} > d_{\min}$ that $\underline{P_r}(d_{\min}, \Delta\omega_\pi(d_{\min})) > \underline{P_r}(d_{\max}, \Delta\omega_\pi(d_{\min}))$ and $\underline{P_r}(d_{\min}, \Delta\omega_\pi(d_{\min})) > \underline{P_r}(d_{\max}, \Delta\omega_\pi(d_{\max}))$, due to the additional path loss between $d_{\min}$ and $d_{\max}$. Combining all of the above observations, we can conclude that one intersection of $\underline{P_r}(d_{\max})$ and g occurs at $\Delta\omega^\star \in [\Delta\omega_\pi(d_{\min}), \Delta\omega_\pi(d_{\max})]$, since $\underline{P_r}(d_{\max})$ is strictly increasing and g strictly decreasing in this interval. For $\Delta\omega < \Delta\omega^\star$, it follows that $\min\{\underline{P_r}(d_{\max}), g\}$ is increasing, while it is decreasing for $\Delta\omega > \Delta\omega^\star$. Hence, the maximum of $\min\{\underline{P_r}(d_{\max}), g\}$ occurs at the intersection $\Delta\omega^\star$.

Appendix D
Proof of Lemma 4

The rate R_2 from (19) can be reformulated as

$$R_2 = \frac{B}{2}\log_2\left(1 + \frac{P_{r,1}(\omega_1) + P_{r,2}(\omega_2)}{FN_0\frac{B}{2}} + \frac{P_{r,1}(\omega_1)P_{r,2}(\omega_2)}{\left(FN_0\frac{B}{2}\right)^2}\right).$$

The product of the individual receive powers $P_{r,i}(\omega_i)$ from (3) can be lower bounded by

$$\begin{aligned} P_{r,1}(\omega_1)P_{r,2}(\omega_2) &\geq \left(\frac{P_t}{2\omega_1\omega_2}\right)^2\left(\frac{c}{2}\right)^4\left(\frac{1}{\ell} - \frac{1}{\tilde{\ell}}\right)^4 \\ &\overset{(a)}{\geq} \left(\frac{P_t}{2\omega_1\omega_2}\right)^2\left(\frac{c}{2}\right)^4\left(\frac{1}{\ell} - \frac{1}{\tilde{\ell}}\right)^4\Bigg|_{d=d_{\max}}, \end{aligned}$$

where (a) follows from the fact that $\frac{1}{\ell} - \frac{1}{\tilde{\ell}}$ is a decreasing in function in the distance d, thus, the lowest value is achieved at the maximum distance $d_{\max}$. Combining this with the noise power leads to the offset α from (21)

$$\alpha = \left(\frac{1}{FN_0\frac{B}{2}}\right)^2\left(\frac{P_t}{2\omega_1\omega_2}\right)^2\left(\frac{c}{2}\right)^4\left(\frac{1}{\ell} - \frac{1}{\tilde{\ell}}\right)^4\Bigg|_{d=d_{\max}}.$$

With the monotonicity of the logarithm, this already establishes the relation

$$R_2 \geq \frac{B}{2}\log_2\left(1 + \alpha + \frac{P_{r,1}(\omega_1) + P_{r,2}(\omega_2)}{FN_0\frac{B}{2}}\right).$$

From this, it also follows directly that

$$\min_{d\in[d_{\min},d_{\max}]} R_2 \geq \frac{B}{2}\log_2\left(1 + \alpha + \frac{2}{FN_0B}\min_{d\in[d_{\min},d_{\max}]} P_{r,1}(\omega_1) + P_{r,2}(\omega_2)\right).$$

Due to the monotonicity of the logarithm, the minimum rate is maximized when the argument is maximized, i.e.,

$$\max_{\Delta\omega}\min_{d\in[d_{\min},d_{\max}]} R_2 \geq \frac{B}{2}\log_2\left(1 + \alpha + \frac{2}{FN_0B}\max_{\Delta\omega}\min_{d\in[d_{\min},d_{\max}]} P_{r,1}(\omega_1) + P_{r,2}(\omega_2)\right).$$

The solution to the inner problem on the right-hand side is given by Theorem 2. Hence, we can also apply it for worst-case design of the sum rate R_2.

The minimum sum receive power by Theorem 2 is given as $\underline{P_r}(d, \Delta\omega^\star)$, which in turn leads to the lower bound on the achievable rate

$$R_2 \geq \underline{R_2} = \frac{B}{2}\log_2\left(1 + \alpha + \frac{\underline{P_r}(d, \Delta\omega^\star)}{FN_0\frac{B}{2}}\right),$$

which is (20) and concludes the proof.

References

[1] W. Saad, M. Bennis, and M. Chen, "A vision of 6G wireless systems: Applications, trends, technologies, and open research problems," *IEEE Network*, vol. 34, no. 3, pp. 134–142, May 2020. DOI: 10.1109/MNET.001.1900287. arXiv: 1902.10265 [cs.IT].

[2] J. Park, S. Samarakoon, H. Shiri, M. K. Abdel-Aziz, T. Nishio, A. Elgabli, and M. Bennis, "Extreme ultra-reliable and low-latency communication," *Nature Electronics*, vol. 5, no. 3, pp. 133–141, Mar. 2022. DOI: 10.1038/s41928-022-00728-8. arXiv: 2001.09683 [cs.IT].

[3] M. Bennis, M. Debbah, and H. V. Poor, "Ultrareliable and low-latency wireless communication: Tail, risk, and scale," *Proceedings of the IEEE*, vol. 106, no. 10, pp. 1834–1853, Oct. 2018. DOI: 10.1109/JPROC.2018.2867029. arXiv: 1801.01270 [cs.IT].

[4] F. Haber and M. Noorchashm, "Negatively correlated branches in frequency diversity systems to overcome multipath fading," *IEEE Transactions on Communications*, vol. 22, no. 2, pp. 180–190, Feb. 1974. DOI: 10.1109/TCOM.1974.1092173.

[5] K.-L. Besser and E. A. Jorswieck, "Reliability bounds for dependent fading wireless channels," *IEEE Transactions on Wireless Communications*, vol. 19, no. 9, pp. 5833–5845, Sep. 2020. DOI: 10.1109/TWC.2020.2997332. arXiv: 1909.01415 [cs.IT].

[6] K.-L. Besser, P.-H. Lin, and E. A. Jorswieck, "On fading channel dependency structures with a positive zero-outage capacity," *IEEE Transactions on Communications*, vol. 69, no. 10, pp. 6561–6574, Oct. 2021. DOI: 10.1109/TCOMM.2021.3097755. arXiv: 2102.02541 [cs.IT].

[7] R. J. Weiler, M. Peter, W. Keusgen, A. Kortke, and M. Wisotzki, "Millimeter-wave channel sounding of outdoor ground reflections," in *2015 IEEE Radio and Wireless Symposium (RWS)*, (San Diego, CA, USA), IEEE, Jan. 2015, pp. 95–97. DOI: 10.1109/RWS.2015.7129712.

[8] J. Naganawa, K. Morioka, J. Honda, N. Kanada, N. Yonemoto, and Y. Sumiya, "Antenna configuration mitigating ground reflection fading on airport surface for AeroMACS," in *2017 IEEE Conference on Antenna Measurements & Applications (CAMA)*, (Tsukuba, Japan), IEEE, Dec. 2017. DOI: 10.1109/cama.2017.8273487.

[9] D. W. Matolak and R. Sun, "Air-ground channel characterization for unmanned aircraft systems: The over-freshwater setting," in *2014 Integrated Communications, Navigation and Surveillance Conference (ICNS) Conference Proceedings*, IEEE, Apr. 2014. DOI: 10.1109/icnsurv.2014.6819996.

[10] ——, "Air-ground channel characterization for unmanned aircraft systems—part I: Methods, measurements, and models for over-water settings," *IEEE Transactions on Vehicular Technology*, vol. 66, no. 1, pp. 26–44, Jan. 2017. DOI: 10.1109/tvt.2016.2530306.

[11] C.-C. Chiu, A.-H. Tsai, H.-P. Lin, C.-Y. Lee, and L.-C. Wang, "Channel modeling of air-to-ground signal measurement with two-ray ground-reflection model for UAV communication systems," in *2021 30th Wireless and Optical Communications Conference (WOCC)*, (Taipei, Taiwan), IEEE, Oct. 2021. DOI: 10.1109/wocc53213.2021.9603250.

[12] C. Sommer, S. Joerer, and F. Dressler, "On the applicability of two-ray path loss models for vehicular network simulation," in *2012 IEEE Vehicular Networking Conference (VNC)*, (Seoul, South Korea), IEEE, Nov. 2012. DOI: 10.1109/vnc.2012.6407446.

[13] A. H. Farzamiyan, M. G. Gaitan, and R. Samano-Robles, "A multi-ray analysis of LOS V2V links for multiple antennas with ground reflection," in *2020 AEIT International Annual Conference (AEIT)*, (Catania, Italy), IEEE, Sep. 2020. DOI: 10.23919/aeit50178.2020.9241147.

[14] K. Guan, G. Li, T. Kürner, A. F. Molisch, B. Peng, R. He, B. Hui, J. Kim, and Z. Zhong, "On millimeter wave and THz mobile radio channel for smart rail mobility," *IEEE Transactions on Vehicular Technology*, vol. 66, no. 7, pp. 5658–5674, Jul. 2017. DOI: 10.1109/TVT.2016.2624504.

[15] W. Khawaja, O. Ozdemir, F. Erden, E. Ozturk, and I. Guvenc, "Multiple ray received power modelling for mmWave indoor and outdoor scenarios," *IET Microwaves, Antennas & Propagation*, vol. 14, no. 14, pp. 1825–1836, Nov. 2020. DOI: 10.1049/iet-map.2020.0046. arXiv: 2001.06459 [eess.SP].

[16] E. Zöchmann, K. Guan, and M. Rupp, "Two-ray models in mmWave communications," in *2017 IEEE 18th International Workshop on Signal Processing Advances in Wireless Communications (SPAWC)*, (Sapporo, Japan), IEEE, Jul. 2017. DOI: 10.1109/SPAWC.2017.8227681.

[17] L. Rapaport, A. Etinger, B. Litvak, G. Pinhasi, and Y. Pinhasi, "Quasi optical multi-ray model for wireless communication link in millimeter wavelengths," *MATEC Web of Conferences*, vol. 210, 03006, 2018. DOI: 10.1051/matecconf/201821003006.

[18] S. Jaeckel, L. Raschkowski, S. Wu, L. Thiele, and W. Keusgen, "An explicit ground reflection model for mm-wave channels," in *2017 IEEE Wireless Communications and Networking Conference Workshops (WCNCW)*, (San Francisco, CA, USA), IEEE, Mar. 2017. DOI: 10.1109/wcncw.2017.7919093.

[19] D. W. Matolak and R. Sun, "Unmanned aircraft systems: Air-ground channel characterization for future applications," *IEEE Vehicular Technology Magazine*, vol. 10, no. 2, pp. 79–85, Jun. 2015. DOI: 10.1109/mvt.2015.2411191.

[20] J. D. Parsons, *The Mobile Radio Propagation Channel*, 2nd ed. Wiley, Nov. 2001. DOI: 10.1002/0470841524.

[21] H. Berger and J. E. Evans, "Diversity techniques for airborne communications in the presence of ground reflection multipath," Massachusetts Institute of Technology, Lincoln Laboratory, Tech. Rep. 1972-27, Sep. 8, 1972.

[22] D. Capriglione, D. Casinelli, and L. Ferrigno, "Use of frequency diversity to improve the performance of RSSI-based distance measurements," in *2015 IEEE International Workshop on Measurements & Networking (M&N)*, (Coimbra, Portugal), IEEE, Oct. 2015. DOI: 10.1109/iwmn.2015.7322973.

[23] E. Basar, "Reconfigurable intelligent surfaces for doppler effect and multipath fading mitigation," *Frontiers in Communications and Networks*, vol. 2, 672857, May 2021. DOI: 10.3389/frcmn.2021.672857. arXiv: 1912.04080 [eess.SP].

[24] K.-L. Besser. (2022). "Ultra-reliability for two-ray ground reflection scenarios, Supplementary material," [Online]. Available: https://github.com/klb2/two-ray-ultra-reliability.

[25] T. S. Rappaport, *Wireless Communications: Principles and Practice*, 2nd ed. Prentice Hall, 2002.

[26] W. C. Jakes, *Microwave Mobile Communications*. Wiley-IEEE Press, 1974.

[27] S. Loyka and A. Kouki, "Using two ray multipath model for microwave link budget analysis," *IEEE Antennas and Propagation Magazine*, vol. 43, no. 5, pp. 31–36, Oct. 2001. DOI: 10.1109/74.979365.

[28] D. Tse and P. Viswanath, *Fundamentals of Wireless Communications*. Cambridge University Press, 2005. DOI: 10.1017/CBO9780511807213.

[29] P. J. Smith, I. Singh, P. A. Dmochowski, J. P. Coon, and R. Green, "Flexible mobility models using stochastic differential equations," *IEEE Transactions on Vehicular Technology*, vol. 71, no. 4, pp. 4312–4321, Apr. 2022. DOI: 10.1109/TVT.2022.3146407.

[30] R. N. Bracewell, *The Fourier Transform and Its Applications*, 3rd ed., ser. McGraw-Hill Series in Electrical and Computer Engineering: Circuits and Systems. McGraw Hill, 2000.

[31] F. W. King, *Hilbert transforms*, ser. Encyclopedia of Mathematics and its Applications 125. Cambridge University Press, 2009, vol. 2. DOI: 10.1017/cbo9780511735271.